Optik - International Journal for Light and Electron Optics 241 (2021) 166883

Contents lists available at ScienceDirect

Optik

journal homepage: www.elsevier.com/locate/ijleo

Original research article

Analysis of lifting scheme based Double Density Dual-Tree Complex Wavelet Transform for de-noising medical images

H. Heartlin Maria [a,*], A. Maria Jossy [a], G. Malarvizhi [a], A. Jenitta [b]

[a] Department of Electronics and Communication Engineering, SRM Institute of Science and Technology, Kattankulathur, Chennai, India
[b] Idhaya Engineering College for Women, Chinnasalem, India

ARTICLE INFO

Keywords:
Image de-noising
DDDT-CWT
Fuzzy
Image enhancement

ABSTRACT

Medical images play a vital role in diagnosis of various diseases. This has paved a path to the extensive use of CT, mammogram, MRI and ultrasound images in the recent days which has caused a rising concern about the radiation dosage that is involved in medical screening process. Owing to this concern low dose screening is widely being performed and has resulted in the introduction of noise, artifacts thus producing low image quality which can adversely affect the judgment of the radiologists. This in turn has led to the demand of enhanced image de-noising techniques. This work is an approach to remove multiple types of noises from low dose medical images using lifting based Double Density Dual-Tree Complex Wavelet Transform (DDDTCWT) and a modified Bernoulli based thresholding technique enhanced by fuzzy optimization technique. The parameters observed from the simulation results of the proposed method were compared with the existing de-noising techniques and results of the proposed method have shown significant improvement over the conventional techniques. The proposed work not only efficiently de-noises the image but also enhances its visual appearance. The Lifting scheme used provides augmented memory for decomposition, thus speeding up the entire de-noising process.

1. Introduction

The presence of noise, artifacts and distortion in the medical images might make the diagnosis highly unstable and unreliable [1]. Noise might decrease the visibility of entities in the image which might result in faulty diagnosis. Noise does not just occur due to low dosage but also due to various other factors like machine specifications, detector specifications, image acquisition, compression and transmission of medical data. Also, low lighting conditions and limited exposure might lead to degradation of the medical data. De-noising is the most essential pre-processing task required for medical investigation and diagnosis [2]. The sole objective of de-noising lies in suppressing noise from the medical image whilst protecting their edge features and textural features. Edge, texture and noise are known as high frequency components thus making it difficult to distinguish them in the process of de-noising and resulting in loss of information. Therefore, often image enhancement techniques are essential post de-noising of medical images. Low Dose CT and mammogram images which are said to be the principal application of CT image technology mainly suffer from additive Gaussian noise. Speckle noise is said to be common in ultra-sound images and MRI images are prone to thermal noise, Rican noise or Poisson noise. Certain cases often result in a mixture of noises which make it even more intractable to remove using a unified de-noising filter as different filters are effective for different type of noise [3].

* Corresponding author.
E-mail address: heartlim@srmist.edu.in (H.H. Maria).

https://doi.org/10.1016/j.ijleo.2021.166883
Received 26 February 2021; Accepted 30 March 2021
Available online 27 April 2021

The flow of the paper goes as follows: Section 2 deals with the literature review of the existing techniques, Section 2 elaborates the methodology of the proposed work, the results and discussion are dealt in Section 4 and Section 5 briefs out the conclusion and future scope.

2. Related work

Numerous researchers have contributed their work in de-nosing over a past period of time with each method having its own advantages and drawbacks [4]. Yang et al. [5] proposed a generative adversarial network with Wasserstein distance and perceptual loss which can de-noise Gaussian noise present in low-dose CT images. The authors have stated that after aggressive de-noising, the visibility of important factors in image has to be compromised. Ji et al. [6] developed a medical image de-noising technique based on biquadratic polynomial with minimum error constraints and low-rank approximation which works based on geometric regularization to suppress Gaussian noise. This method has shown significant improvement with respect to detail preserving with the use of singular value thresholding and like most other methods it can suppress only Gaussian noise.

A modified Haar Wavelet based decomposition with optimized loop was used by Das et al. [1] to de-noise and enhance the fusion images obtained by positron emission tomography (PET) and computed tomography (CT) images. However, Haar wavelet is non-continuous in nature and might result in producing an uneven wave envelope. Chen et al. [7] proposed Discrete Wavelet Transform (DWT) decomposition and modified median filter for de-noising Gaussian noise and impulse noise. Although the observed results proved to be satisfactory, DWT suffers two main drawbacks such as shift variance and aliasing which is in turn overcome by the de-noising technique proposed by Khuram et al. [8] based on Dual Tree Complex Wavelet Transform (DT-CWT). The DT-CWT technique suppressed Gaussian noise to a great extent yet suffered a drawback of data redundancy in the sub bands. Most de-noising techniques were efficient for one type of noise and neural network based de-noising techniques often require to be re-trained for new parameters and different type of noises. Also, the efficiency of the wavelet de-noising depends on the threshold selection which is another important factor.

Be it hard thresholding or soft thresholding technique, each has its own defect and drawbacks over which various attempts were taken by researchers using various techniques to overcome them. Chunli et al. [9] used an adaptive threshold function using exponentiation to meet non stationery and time varying requirements. Jing-yi et al. [10] proposed an improved soft thresholding function known as semi-soft thresholding which involves the use of complex exponential functions which is more adaptable than the previous method. Naveed et al. [11] proposed an optimum threshold tuning method that was executed by differing the threshold value and its function at the optimum decomposition level using a modified type of unified thresholding. Wang et al. [12] identified a more advanced type of thresholding technique where the threshold was selected based on inter-scale correlation factor. Carlos and Khuram et al. [11,19] selected the threshold based of the Probability of False Alarm(PFA). But the use of Empirical Distribution Function(EDF) to compute the PFA was tedious to determine in case of values closer to 0 and 1. In spite of choosing an efficient wavelet transform and a careful threshold selection the visibility of the image is compromised during iterative de-noising techniques. In order to overcome this problem various types of histogram equalization techniques are being used which include a histogram method proposed by Sonal Raj et al. [14] to modify the Probability Density Function(PDF) with padding factors to increase the contrast. An improved histogram equalization technique was proposed by Ali et al. [15] using weighted functions to enhance the details of the important parts

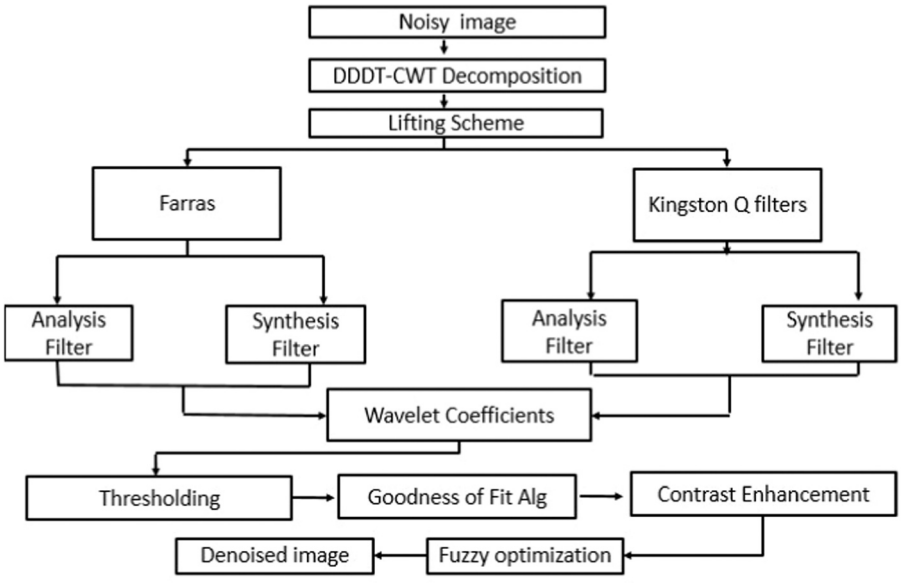

Fig. 1. Flow of proposed Double Density-DTCWT de-noising method.

separately and a sub-image histogram equalization technique proposed by Liyun et al. [16] based on mean and variance.

2.1. Contribution

In order to overcome the existing drawbacks, we have implemented a lifting scheme based DDDT-CWT method in this paper. The lifting scheme not only speeds up the working of the wavelet but also provides augmented virtual memory space for arithmetic operations. The proposed Double Density expansion rectifies the redundancy issue faced by DT-CWT of the existing method. Adding to its advantage, the modified Bernoulli based PFA thresholding technique overcomes the defect of the conventional PFA method thus making it more suitable for clinical trials. Also, the visibility of the image is recovered through the implementation of MSE based dual-histogram equalization technique with fuzzy inference for obtaining optimal results.

3. Proposed methodology

The proposed method is a combination of an improved and efficient de-noising as well as enhancement technique. The flow of proposed DDDTCWT de-noising method is shown in Fig. 1 which consists of three stages namely data pre-processing, data cleansing and enhancement of de-noised image. Data preprocessing involves the addition of 4 types of noises namely additive Gaussian noise, salt and pepper noise, speckle noise and Poisson noise which are said to be common in CT, MRI and ultra-sound images. The middle stage deals with data cleansing which includes the de-noising technique based on DDDTCWT decomposition and Chi-Square Test. The last stage deals with enhancing the de-noised image using a dual histogram equalization method to reconstruct the loss in the visibility of the image and this process is optimized through fuzzy interference.

3.1. Double Density Dual Tree-Complex Wavelet Transform

Complex wavelet transform (CWT) is often used as a substitute to DWT. DDDT-CWT is preferred over DT-CWT as it is found to be more advantageous in terms of data redundancy in the sub bands. Fig. 2 shows that the Double Density DT-CWT is 4 times expansive based on scaling with four different wavelets [17]. Each level is designed such that the first wavelet pair is offset from the other by half and the second pair form an approximate Hilbert Pair. From Fig. 1 we understand that both tree a and tree b consist of analysis and synthesis filters each. Tree a is designed using Farras filter set which is essential to overcome aliasing with near symmetric property that is well suited for reconstruction of the filter bank

$$S(Z) = S_L(Z) + S_H(Z) \tag{1}$$

S_L- low pass filters in tree 1 and 2.
S_H- high pass filters in tree 1and 2

$$S_L(Z) = 1/2\left[C_a^1(z^2)H_0a(z^1) + C_b^1(z^2)H_0b(z^1) + E_a^1(z^2)G_0a(z^1) + E_b^1(z^2)G_0b(z^1)\right] \tag{2}$$

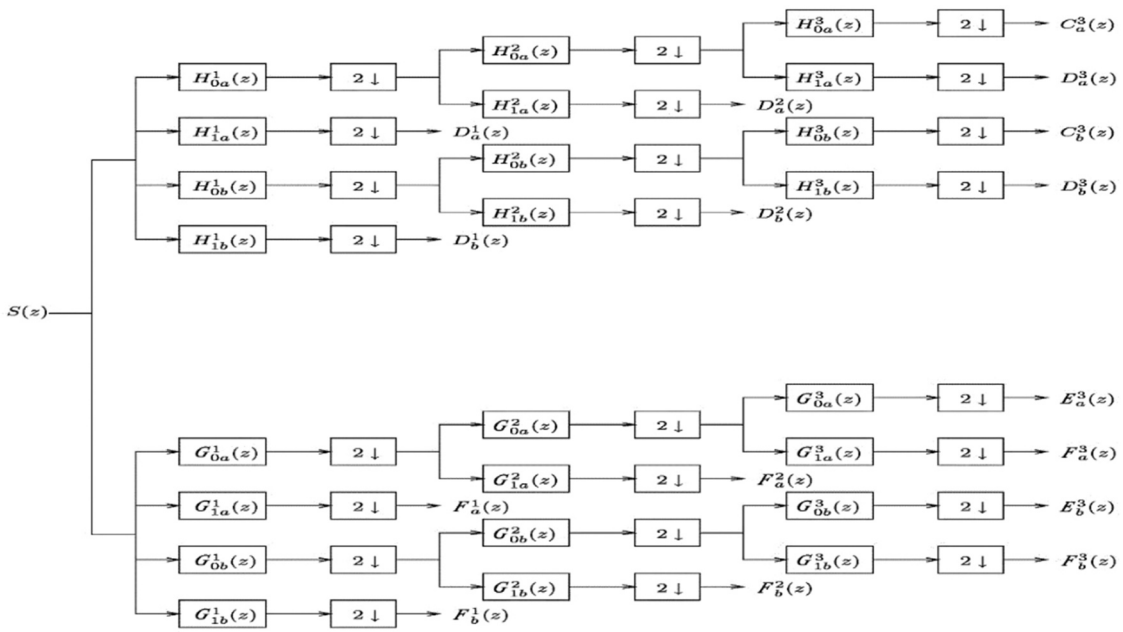

Fig. 2. Representation of Double Density DT-CWT decomposition.

where,

$$\begin{aligned} C_a^1(z^2)H_0a(z^1) &= S(z)\left[H_0(z)H_0(z^1) + H_0(z)H_0(z^1)\right] \\ C_b^1(z^2)H_0b(z^1) &= S(-z)\left[H_0(-z)H_0(z^1) - H_0(-z)H_0(z^1)\right] \\ E_a^1(z^2)G_0a(z^1) &= S(z)\left[H_0(z)H_0(z^1) + H_0(z)H_0(z^1)\right] \\ E_b^1(z^2)G_0b(z^1) &= S(-z)\left[H_0(-z)H_0(z^1) - H_0(-z)H_0(z^1)\right] \\ S_L(z) &= 1/2\left[S(z)H_0(z)H_0(z^1)\right] \end{aligned} \tag{3}$$

Tree b is designed using Kingston Q filters which are shift invariant and commonly used in wavelets constructed with more than one stage. In high pass part, the aliasing term consisting of S(–z) will vanish & the decomposition becomes shift-invariant.

$$S_H(Z) = 1/2\left[D_a^1(z^2)H_1a(z^1) + D_b^1(z^2)H_1b(z^1) + F_a^1(z^2)G_1a(z^1) + F_b^1(z^2)G_1b(z^1)\right] \tag{4}$$

where,

$$\begin{aligned} D_a^1(z^2)H_1a(z^1) &= S(z)\left[H_0(z)H_0(z^1) + H_0(z)H_0(z^1)\right] \\ D_b^1(z^2)H_1b(z^1) &= S(-z)\left[H_0(-z)H_0(z^1) - H_0(-z)H_0(z^1)\right] \\ F_a^1(z^2)G_1a(z^1) &= S(z)\left[H_0(z)H_0(z^1) + H_0(z)H_0(z^1)\right] \\ F_b^1(z^2)G_1b(z^1) &= S(-z)\left[H_0(-z)H_0(z^1) - H_0(-z)H_0(z^1)\right] \\ S_H(Z) &= \frac{1}{2}\left[S(z)H_0(z)H_0(z^1) + H_0(z)H_0(z^1)\right] \end{aligned} \tag{5}$$

Therefore,

$$S_H(z) = 1/2\left[S(z)H_0(z)H_0(z^1) + H_0(z)H_0(z^1)\right] + \left[S(z)H_0(z)H_0(z^1)\right] \tag{6}$$

3.2. PFA based Bernoulli thresholding technique

This work is comprised of PFA based thresholding technique incorporated with Bernoulli Distribution function and Gaussian probability density function for improved performance. The PFA based thresholding technique is a type of soft thresholding technique [11,13]. Soft thresholding is preferred over hard thresholding as edge features might tend to be lost during the process. BDF is preferred over EDF as EDF is not suitable for value closer to 0 and 1 whereas BDF is well suited for clinical trials and research purposes. The mathematical expression of BDF based PFA thresholding technique is given as,

$$\mathrm{PFA} = \int \left\{ \mathrm{U_k(n)(t); \Delta jk} > \lambda \middle| \hat{\mathrm{H}} \right\} \mathrm{D\hat{Y}(z)} \Big/ \mathrm{dz \cdot du_k}^{\Psi}(\mathrm{t}) \tag{7}$$

where,

$U_k\ (n)(t)$ is the noise co-efficient $\int\{\mathrm{U_k(n)(t); \Delta jk} > \lambda|\widehat{\mathrm{H}}\}$ represents the detection of the range of co-efficients. $\mathrm{d\hat{Y}(z)/dz}$ represents the PDF.

The Gaussian PDF is given by,

$$\hat{\mathrm{Y}} = \frac{1}{\sigma\sqrt{2\pi}} exp^{-1/2(x-\mu/\sigma)^2} \tag{8}$$

where,

ᴍ is the mean of the noisy co-efficients and σ represents the standard deviation of the noisy co-efficients. The noisy co-efficients are identified by skewness of Bernoulli Distribution function which is given by,

Table 1
Observed values of Threshold vs. PFA at four levels of decomposition.

Level-1		Level-2		Level-3		Level-4	
Threshold	PFA	Threshold	PFA	Threshold	PFA	Threshold	PFA
0	1	0	1	0	1	0	1
8.5	1	8.5	1	8.5	0.99923	8.5	1
9	0.99999	9	1	9	0.99885	9	1
9.5	0.99952	9.5	0.99962	9.5	0.99769	9.5	0.99885
10	0.99894	10	0.99936	10	0.99692	10	0.99769
20	0.71501	20	0.81546	20	0.81944	20	0.83333
30	0.4381	30	0.4380	30	0.36806	30	0.47917

$$U_k(n)(t) = \Upsilon_1$$

where, Υ_1 represents skew.

$$\Upsilon_1 = \frac{E[(X - E(X)]}{\sqrt{Var[X])]3}} \tag{9}$$

'X' represents mean of the range of co-efficients. E[X] represents median of the range of co-efficients. $\sqrt{}$Var[X] represents Standard Deviation of the range of co-efficients. Uk(n)(t) is the noise co-efficient divided into 'M' windows having size 'L + 1'. Candidate threshold 'λ' is applied to the co-efficients on each window. For each 'λ', the PFA is computed and recorded. Then the accumulated PFA is divided by the total No. of windows 'M'. In general, higher number of false alarms are observed for low 'λ' and vice-versa (Table 1).

3.3. Lifting

Lifting scheme is a process used mainly in designing new wavelets or alongside existing wavelets in order to improve its working efficiency. A wavelet transform with a lifting scheme is otherwise known as a second generation wavelet [17]. Lifting scheme involves three phases namely the split phase which splits the odd and even co-efficients based on their index value, predict phase which enables polynomial cancellation in high pass co-efficients and the update phase that updates the even set to a certain scaling function [18] (Fig. 3).

3.4. Chi-square test (CST)

CST [8] is often used to compare and analyze the difference between the observed experimental values and the existing theoretical values with the following steps,

- Let O denote the observed value and E denote the expected value.
- Calculate X^2 = (O–E)/E.
- Calculate the Degree of freedom 'D' = (Columns-1) (Rows-1).
- Obtain the significance level from X^2 across D in the Chi-Square Distribution table.
- If the calculated X^2 is greater than the tabular X^2 then, this case is known as alternate hypothesis.

3.5. Dual histogram equalization based on adaptive sigmoid function

The de-noised images are likely to be affected by low visibility and loss of information. Hence, an efficient image enhancement technique is required to enhance and restore the features of the de-noised image to a certain extent. The Bi-histogram technique equalizes the histogram of the de-noised image using adaptive sigmoid function which in turn enhances the appearance of the de-noised image adversely [16]. The proposed Dual Equalization with Adaptive Sigmoid Function (DEASF) splits the histogram of the image into two sub histograms known as the upper histogram and lower histogram. The mean of the image and the PDF of the histogram are computed after which the CDF is computed which in turn facilitates the generation of the upper sigmoid function and the lower sigmoid function of the upper histogram and the lower histogram respectively. The mathematical explanation of the bi-histogram method is as follows:

$$\int_{q_0}^{q} G(s)ds = \int_{p_0}^{p} H(s)ds \tag{11}$$

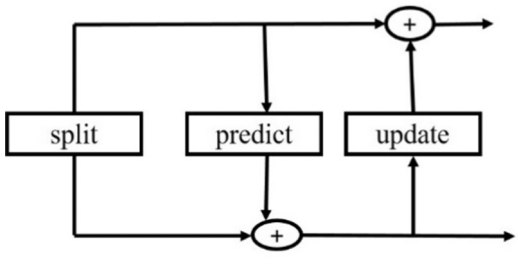

Fig. 3. Diagrammatic representation of the phases in lifting scheme [18].

$$\int_{q_0}^{q}\left[\left[N_1^2/(q_k-q_0)+N_2^2/(q_k-q_0)\right]\right]\mathrm{ds}=\int_{q_0}^{p}H(s)ds$$
$$\left[N_1^2/(q-q_0)+N_2^2/(q-q_0)\right]\Big/ q_k-q_0=\int_{q_0}^{p}H(s)ds \tag{12}$$
$$\left[N_1^2/(q-q_0)+N_2^2/(q-q_0)\right]\Big/ q_k-q_0=\int_{q_0}^{p}H(s)ds$$

where,

H(p) is the histogram of N × N image with gray levels p = (p_0,p_k). The monotonic pixel brightness transformation is to be obtained such that the desired output histogram G(q) is uniform over the whole output brightness scale q = (q_0, q_k).

3.6. Fuzzy optimization

Optimization techniques are used to maximize the efficiency of any algorithm iteratively until the optimum satisfactory result is obtained. The proposed system deploys the Darwin's Particle Swarm Optimization technique(DPSO) shown in Fig. 4 to improve the working efficiency of the image enhancement stage. The swarm size η_s which is otherwise known as the number of particles in the swarm is initialized. The larger the swarm size, larger parts of the search space would be covered per iteration. Also, if the particle size is larger a suitable solution might be obtained earlier with less number of iterations. The acceleration co-efficients C_1, C_2 and the random vectors R_1, R_2 are then initialized. c_1 and c_2 are also known as trust parameters where C_1 denotes the confidence the particle has in itself and C_2 is the confidence of the particle on its neighbors.

The number of iterations is set to N = 50 after sample trials and the Global best (Gbest) otherwise known as the existing best value and Personal best (Pbest) which is the alternate "best" value that is tracked by the particle swarm optimizer as the best value are updated [23]. The Response surface methodology (RSM) fitness function is used to map the particles to a real value close to the optimization criterion. The optimization algorithm helps in yielding a satisfactory and optimum result [22,23].

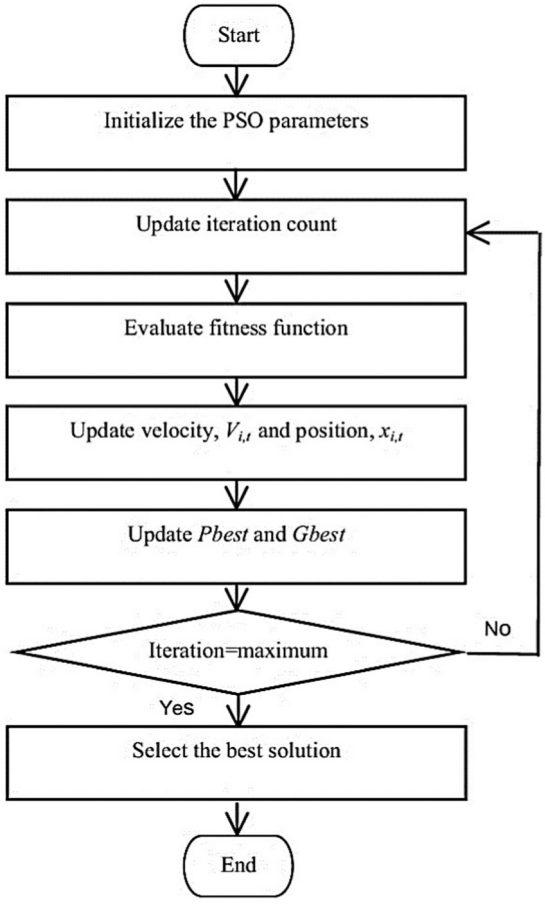

Fig. 4. Flow of fuzzy optimization algorithm [23].

4. Results and discussion

4.1. Experimental setup

We have used four kinds of medical dataset for different types of noises. Brain MRI dataset is used for Poisson noise, ovarian CT images for additive Gaussian noise, artery ultra sound images for speckle noise and mammogram dataset for mixture of noise types. The datasets were collected from wikicancerarchive.net [24]. The images were primarily in DICOM format which were retrieved using NBIA (National Bio-medical Image Archive) data retriever and then were converted to tiff format for convenience. We collected 1400 datasets of ovarian set resized to 512 × 512, 100 artery ultrasound datasets, 100 mammogram datasets and 70 MRI datasets for processing resized to 256 × 256.

4.2. Results of simulation and comparative analysis

To felicitate a quantitative performance, the following metrics have been used such as Peak signal to noise ratio(PSNR), Structural similarity (SSIM), Mean Absolute Error (MAE), image enhancement factor(IEF). Fig. 5 shows the subjective visual results of the CT image of Stage IV ovarian Cancer. Since Gaussian noise is commonly present in CT images, it is added to the input CT-img1 at a noise intensity $\sigma = 15$. This is done in order to show the efficiency of the proposed de-noising at higher noise intensity levels. The de-noised image obtained as an output of the proposed double density DT-CWT is free from noise and artifacts but the visibility of the image seems to have reduced due to intensive wavelet decomposition process. Therefore, to improve the visibility that had been previously compromised, a bi-histogram equalization technique based on adaptive sigmoid functions was introduced. This equalization technique was further optimized using fuzzy optimization method.

The final output of Fig. 5 is the de-noised image with enhanced visibility which is well suited for diagnostic purposes. The same process has been followed for Figs. 6 and 7 which are the follow up CT images of the same person affected with stage IV ovarian cancer. The same noise intensity $\sigma = 15$ was preferred for all CT images for comparative analysis. Table 2 consists of the observed parametric values of the de-noised CT images. From Figs. 8–10 we have used MRI images of the brain. Images of different modalities containing different noises have been examined and analyzed using the proposed de-noising technique to understand its efficiency. Since poisson noise is most common in MRI images, we have generated poisson noise from the data instead of adding artificial noise to the data. The image with the generated poisson noise is then de-noised and enhanced using double density DT-CWT and fuzzy optimized histogram equalization. The parametric values observed from the de-noised MRI images are tabulated in Table 3. From the observed values it is inferred that the PSNR values of the de-noised MRI data is evidently high. Similarly, two other noise modalities such as ultrasound and mammography were collected and de-noised and the results were tabulated. The subjective de-noising results of ultrasound images of the artery containing generated speckle noise of intensity $\sigma = 0.5$ is displayed from Figs. 11–13. The observed parametric values are tabulated in Table 4. The fourth modality is mammogram and in this dataset, two types of noises are added in order to show the effect of the proposed de-noising on multiple types of noises. The de-noising results of mammogram images with added Gaussian noise of intensity $\sigma = 10$ as well as salt and pepper noise of intensity $\sigma = 0.1$ is shown from Figs. 14–16. The respective parametric values observed are tabulated in Table 5.

The proposed de-noising is also compared with existing wavelet based de-noising techniques and the simulation results are shown in Fig. 18. The parametric values observed are displayed in Table 6 and it is inferred that the PSNR and SNR of proposed de-noising has shown significant improvement over the existing wavelet transforms. The results of the various image modalities are also compared with the similar image modalities discussed in the literature review [7] and the results are displayed in Table 7. From the results it is inferred that the proposed de-noising has shown around 50–55% increase in PSNR values of low noise images when compared to existing wavelet based de-noising techniques. It is significant that the proposed de-noising has shown a vast improving in the PSNR and SNR values comparatively. The results of the histogram of the ovarian CT image before and after equalization is also provided in Fig. 17 and it is visually evident that the histogram of the image after enhancement is equalized compared to the histogram of the image before enhancement (Fig. 18).

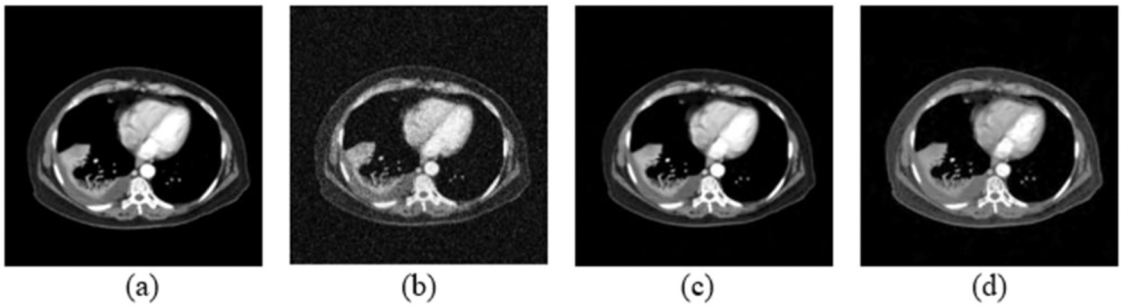

Fig. 5. Shows (a) input image CT-img1 (b) addition of Gaussian noise to the input image (c) De-noised image using proposed de-noising technique (d) Fuzzy optimized enhanced output image.

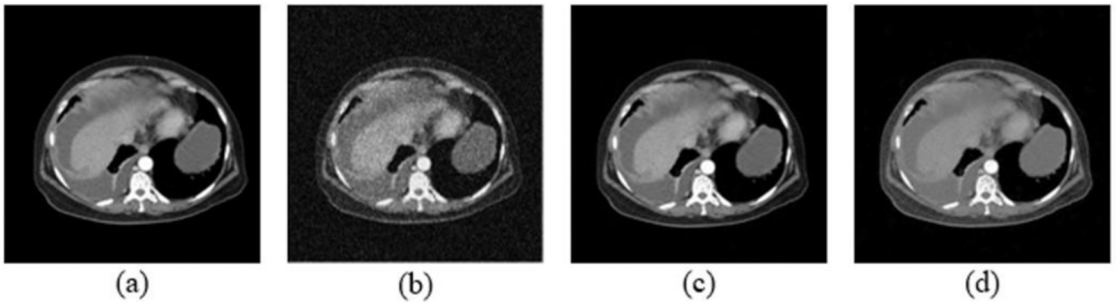

Fig. 6. Shows (a) input image CT-img2 (b) addition of Gaussian noise to the input image (c) De-noised image using proposed de-noising technique (d) Fuzzy optimized enhanced output image.

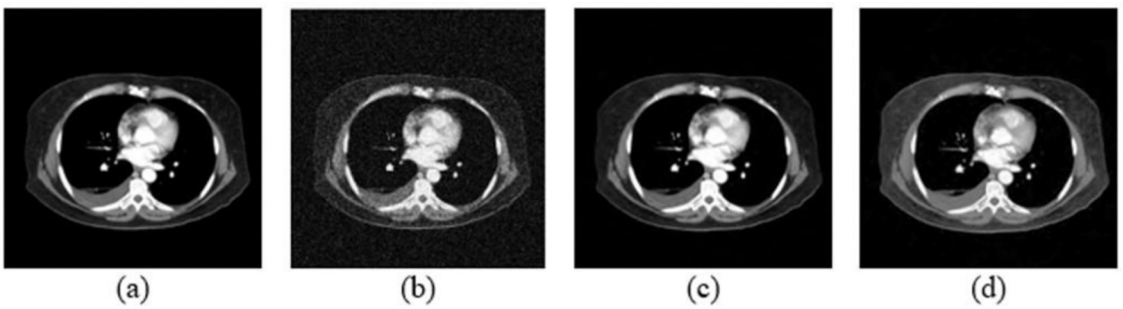

Fig. 7. Shows (a) input image CT-img3 (b) addition of Gaussian noise to the input image (c) De-noised image using proposed de-noising technique (d) Fuzzy optimized enhanced output image.

Table 2
Observed parametric values of CT images.

	Noise intensity	PSNR	SSIM	IEF	MAE	SNR
CT-img1	15	34.0143	0.0226	8.7478	2.7788	19.8977
CT-img2	15	33.6006	0.2353	7.9319	2.8457	19.0711
CT-img3	15	33.1947	0.2336	7.1899	2.9927	18.2583
CT-img4	15	34.7825	0.2658	7.1154	2.1515	19.2047
CT-img5	15	34.1035	0.2147	8.1241	1.0238	18.3698
Average		33.9391	0.1944	7.8218	2.3585	18.9603

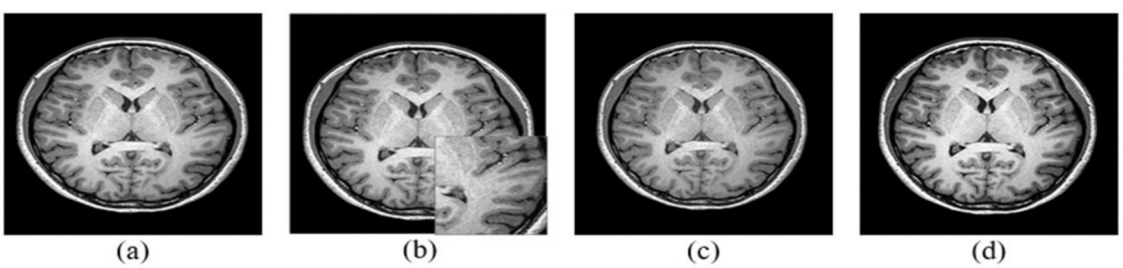

Fig. 8. Shows (a) input image MRI-1 (b)addition of poisson noise to the input image (c) De-noised image using proposed de-noising technique (d) Fuzzy optimized enhanced output image.

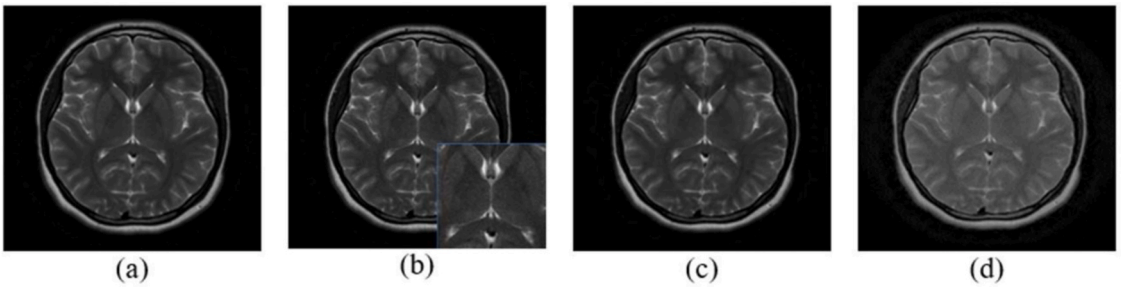

Fig. 9. Shows (a) input image MRI-2 (b) addition of poisson noise to the input image (c) De-noised image using proposed de-noising technique (d) Fuzzy optimized enhanced output image.

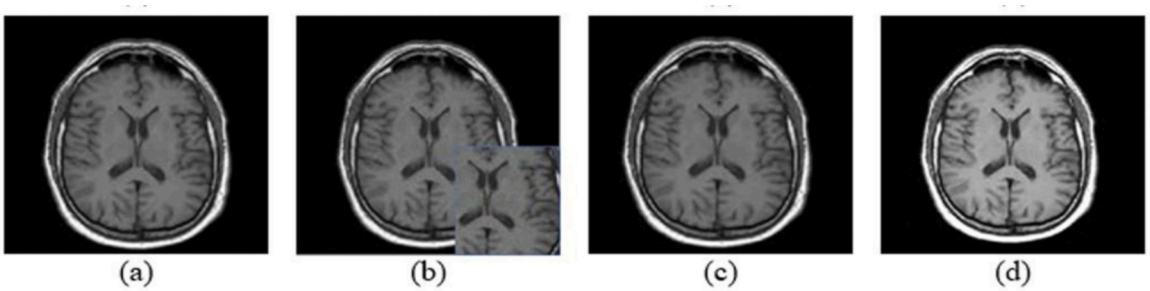

Fig. 10. Shows (a) input image MRI-3 (b) addition of poisson noise to the input image (c) De-noised image using proposed de-noising technique (d) Fuzzy optimized enhanced output image.

Table 3
Observed parametric values of MRI images.

	Noise intensity	PSNR	SSIM	IEF	MAE	SNR
MRI-1	0.05	46.0212	0.3561	19.0038	1.8897	34.2159
MRI-2	0.05	46.4242	0.2658	19.3811	1.6589	35.0035
MRI-3	0.05	46.2010	0.3325	18.0384	1.9984	34.1058
MRI-4	0.05	45.2121	0.3398	19.8759	1.6781	34.6899
MRI-5	0.05	46.2010	0.3579	18.0384	1.3644	34.7654
Average		46.0119	0.3304	18.8675	1.7179	34.5561

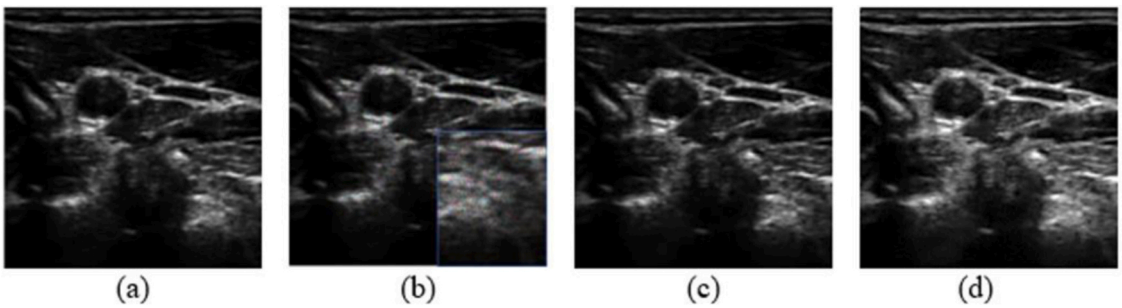

Fig. 11. Shows (a) input image MRI-3 (b) addition of speckle noise to the input image (c) De-noised image using proposed de-noising technique (d) Fuzzy optimized enhanced output image.

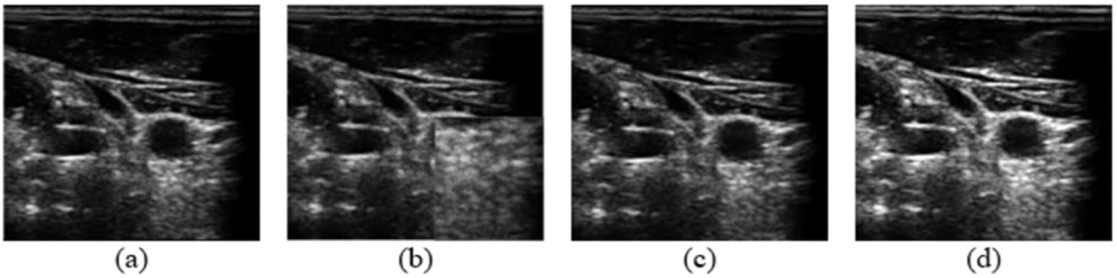

Fig. 12. Shows (a) input image MRI-3 (b) addition of speckle noise to the input image (c) De-noised image using proposed de-noising technique (d) Fuzzy optimized enhanced output image.

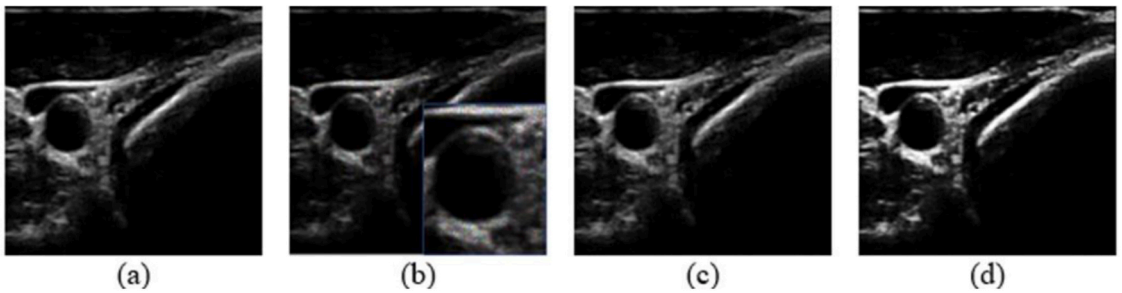

Fig. 13. Shows (a) input image MRI-3 (b) addition of speckle noise to the input image (c) De-noised image using proposed de-noising technique (d) Fuzzy optimized enhanced output image.

Table 4
Observed parametric values of ultrasound images.

	Noise intensity	PSNR	SSIM	IEF	MAE	SNR
Ultra sound-1	0.05	44.5857	0.4167	11.0940	2.0940	33.7285
Ultrasound-2	0.05	44.1025	0.3518	12.0356	2.1020	34.9821
Ultrasound-3	0.05	43.3351	0.3611	11.2533	1.0398	34.6352
Ultrasound-4	0.05	44.1102	0.3258	12.5874	1.8975	33.1248
Ultrasound-5	0.05	44.1002	0.3215	12.2586	1.0035	35.0254
Average		44.0467	0.3553	11.8457	1.6273	34.2992

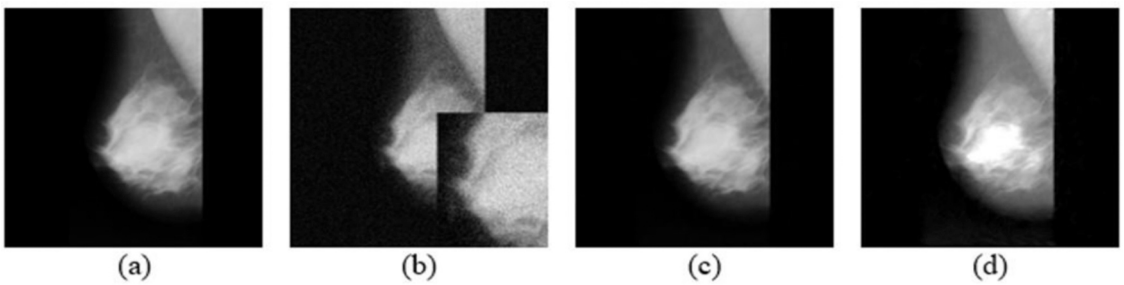

Fig. 14. Shows (a) input image Mamo-1 (b) addition of Gaussian and salt & pepper noise to the input image (c) De-noised image using proposed de-noising technique (d) Fuzzy optimized enhanced output image.

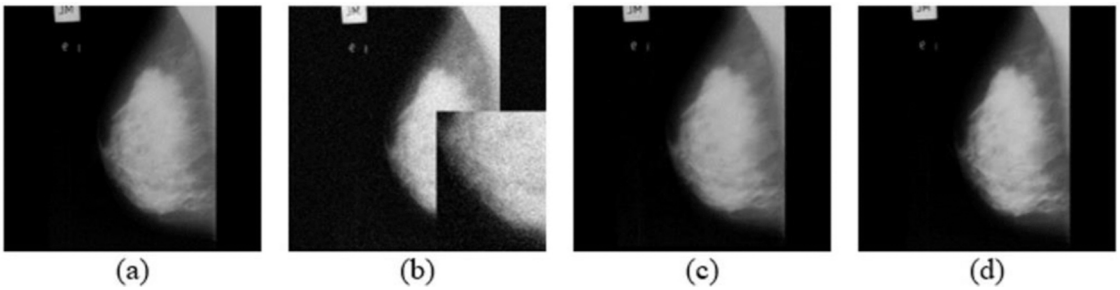

Fig. 15. Shows (a) input image Mamo-2 (b) addition of Gaussian and salt & pepper noise to the input image (c) De-noised image using proposed de-noising technique (d) Fuzzy optimized enhanced output image.

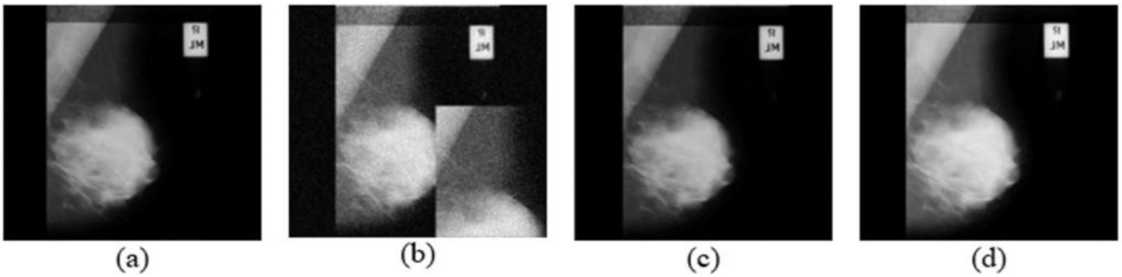

Fig. 16. Shows (a) input image Mamo-3 (b) addition of Gaussian and salt & pepper noise to the input image (c) De-noised image using proposed de-noising technique (d) Fuzzy optimized enhanced output image.

Table 5
Observed parametric values of mammogram images.

	Gaussian/S&P	PSNR	SSIM	IEF	MAE	SNR
Mamo-1	10/0.1	42.2051	0.0259	19.6030	1.0863	33.3963
Mamo-2	10/0.1	40.4100	0.3143	17.0080	1.3816	33.5512
Mamo-3	10/0.1	41.2519	0.2541	18.2511	1.2584	33.0548
Mamo-4	10/0.1	42.2245	0.2128	18.0358	1.0368	33.1068
Mamo-5	10/0.1	40.8670	0.2953	18.7420	1.2949	33.1021
Average		41.3917	0.2204	18.3279	1.2116	33.2422

Table 6
Comparison chart of observed parametric values of conventional wavelet de-noising and proposed de-noising.

	DWT [17,18,21]	SWT [20]	HAAR [19]	DD-DTCWT
MAE	0.7076	4.4444	3.5497	0.6101
PSNR	43.6983	27.5071	27.7929	45.7796
SSIM	0.9626	0.2888	0.5421	0.9643
SNR	39.2657	16.4492	7.4549	43.4284
IEF	3.8909	0.9999	1.0008	5.6187

Table 7
PSNR comparison of the proposed de-noising with existing de-noising techniques.

Image modality	Sigma value	Contourlet [7]	DT-CWT [7]	Coupling de-noising [7]	Proposed DDDTCWT
CT	0.05	21.1413	20.1149	24.7744	47.1022
MRI	0.05	21.1941	21.6879	24.7165	46.0119
Ultra-sound	0.05	20.4370	20.4454	23.8070	44.0467

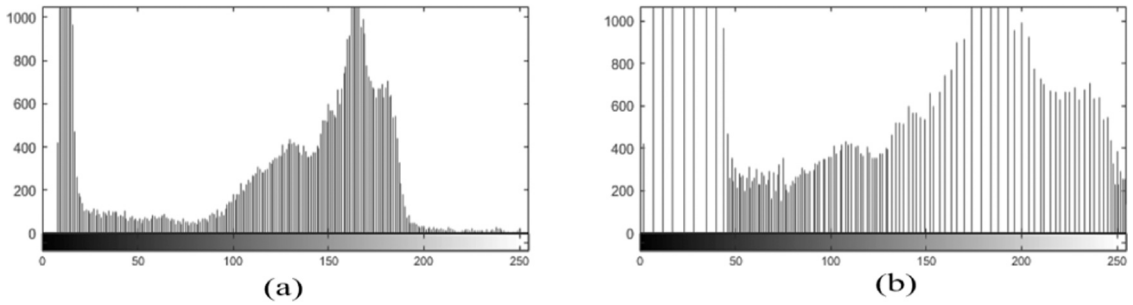

Fig. 17. Histogram before and after equalization and fuzzy optimization (a) Histogram of de-noised image (b) Histogram of enhanced image.

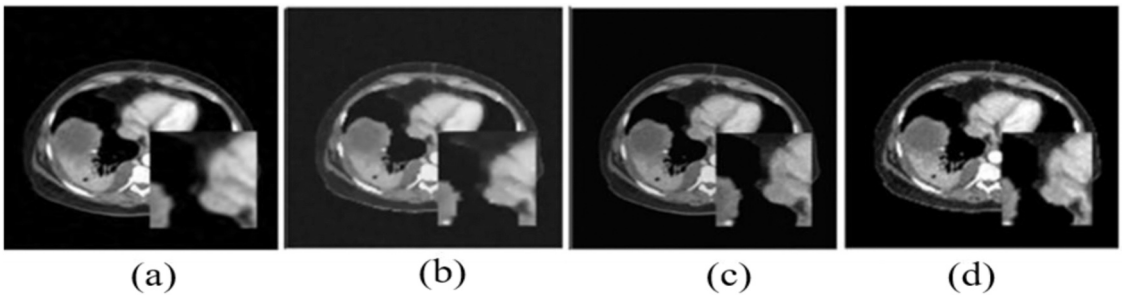

Fig. 18. Simulation results of (a) DWT (b)Haar (c) Stationery (d) proposed DD-DTCWT.

4.3. Discussion

The proposed de-noising works well on Gaussian, Poisson, speckle and salt and pepper noises. Also, the proposed method is efficient on de-noising mixture of noises which is a tedious task in most cases. The enhancement phase ensures that the visibility of the medical image is not compromised which is another added advantage of this work, as the sole objective of de-noising is not just removal of the noise but also retaining the information in the image.

5. Conclusion

In this paper, we have proposed a medical image de-noising method from the image decomposition perspective. Contradictory to most existing works, this method deals with removing multiple noises rather than just one type of noise. The proposed work not only focuses on de-noising the image but also enhancing the de-noised image so as to retain the visibility of the image which is also quite a challenge in most conventional de-noising techniques as they suffer loss in visibility of the de-noised image which might not be suitable for precise diagnosis. In future, the work can be carried out using real time images of other image modalities and other forms of noises that are observed in medical data.

Compliance with ethical standards

This work is performed using publicly available medical image dataset. Therefore, formal consent is not required for this study type. This article does not contain any studies with human participants performed by any of the authors.

Funding

This work was not funded.

Declaration of Competing Interest

The authors declare no conflict of interest over this work.

References

[1] K. Das, M. Maitra, M. Banerjee, P. Sharma, Embedded implementation of early started hybrid denoising technique for medical images with optimized loop, emerging technology in modelling and graphics, Adv. Intell. Syst. Comput. 937 (2020) 295–308.
[2] T. Aravindan, R. Seshasayanan, Denoising brain images with the aid of discrete wavelet transform and monarch butterfly optimization with different noises, J. Med. Syst. 42 (11) (2018) 1–13.
[3] Y. Chang, L. Yan, M. Chen, H. Fang, S. Zhong, Two-stage convolutional neural network for medical noise removal via image decomposition, IEEE Trans. Instrum. Meas. 69 (2020) 2707–2721.
[4] L. Fan, F. Zhang, H. Fan, Brief review of image denoising techniques, Vis. Comput. Ind. Biomed. Art. 20 (2019), 481-480.
[5] Q. Yang, P. Yan, Y. Zhang, H. Yu, Y. Shi, X. Mou, M.K. Kalra, Y. Zhang, L. Sun, G. Wang, Low-dose CT image denoising using a generative adversarial network with wasserstein distance and perceptual loss, IEEE Trans. Med. Imaging 37 (2018) 1348–1357.
[6] L. Ji, Q. Guo, M. Zhang, Medical image denoising based on biquadratic polynomial with minimum error constraints and low-rank approximation, IEEE Access 8 (2020) 84950–84960.
[7] B. Chen, J. Cui, Q. Xu, et al., Coupling denoising algorithm based on discrete wavelet transform and modified median filter for medical image, J. Cent. South Univ. 26 (2019) 120–131.
[8] K. Naveed, B. Shaukat, N. Rehman, Dual tree complex wavelet transform-based signal denoising method exploiting neighbourhood dependencies and goodness-of-fit test, R. Soc. Open Sci. 5 (2018), 180436.
[9] W. Chunli, Z. Chunlei, Z. Pengtu, Denoising algorithm based on wavelet adaptive threshold, in: International Conference on Applied Physics and Industrial Engineering, vol. 24, Elsevier, 2012, pp. 678–685.
[10] L. Jing-yi, L. Hong, Y. Dong, Z. Yan-sheng, A new wavelet threshold function and denoising application, Math. Probl. Eng. 2016 (2016) 1–8.
[11] K. Naveed, M. Akhtar, M. Siddiqui, N. Rehman, A statistical approach to signal denoising based on data-driven multiscale representation, Electr. Eng. Syst. Sci. (2020).
[12] R. Wang, A new wavelet threshold determination method considering interscale correlation in signal denoising, Math. Probl. Eng. (2015).
[13] C. Mello, A. Sanchez, A. Oliveira, A. Lopes, An efficient gray-level thresholding algorithm for historic document images, J. Cult. Heritage 9 (2008) 109–116.
[14] S. Raj, S. Raj, S. Kumar, Laboratory surveillance for SARS-CoV-2 in India: performance of testing & descriptive epidemiology of detected COVID-19, January 22 – April 30, 2020, Indian J. Med. Res. 151 (2020) 424–437.
[15] M.M.N. Ali, M. Abdullah-Al-Wadud, Image enhancement using a modified histogram equalization. Communications in Computer and Information Science, Springer, 2012.
[16] L. Zhuang, Adaptive Image enhancement using entropy-based subhistogram equalization, Comput. Intell. Neurosci. (2018) 1–13.
[17] R. Srivastava, C. Patil, R. Mishra, Implementation of Dual Tree and Double Density Complex Wavelet Transform in Verilog HDL, J. Eng. Res. Appl. (2018) 51–56.
[18] A. Safari, Y. Kong, The application of lifting DWT in digital image processing. Advances in Mechanical and Electronic Engineering, Springer, 2013.
[19] A. Kumar, H. Tomar, V.K. Mehla, R. Komaragiri, M. Kumar, Stationary wavelet transform based ECG signal denoising method, ISA Trans. (2020).
[20] J. Pang, Improved image denoising based on Haar wavelet transform, in: IEEE SmartWorld, Ubiquitous Intelligence & Computing, Advanced & Trusted Computed, Scalable Computing & Communications, Cloud & Big Data Computing, Internet of People and Smart City Innovation (SmartWorld/SCALCOM/UIC/ATC/CBDCom/IOP/SCI), 2017, pp. 1–6.
[21] P. Bhargava, S. Choubey, R. Bhujade, N. Jain, Image denoising using discrete wavelet transform: a theoretical framework, Int. J. Eng. Technol. 7 (2018) 120.
[22] R.C. Eberhart, Y. Shi, Particle swarm optimization: development, applications and resources, in: Proceedings of the IEEE Conference on Evolutionary Computation, ICEC, 2001.
[23] U.K. Acharya, S. Kumar, Particle swarm optimized texture based histogram equalization (PSOTHE) for MRI brain image enhancement, Optik 224 (2020), 165760.
[24] L. Beer, H. Sahin, I. Blazic, H.A. Vargas, H. Veeraraghavan, J. Kirby, B. Fevrier-Sullivan, J. Freymann, C. Jaffe, T. Conrads, G. Maxwell, K. Darcy, E. Huang, E. Sala, Study of orthophosphate, pyrophosphate, and pyrophosphatase in saliva with reference to calculus formation and inhibition, J. Periodontol. 82 (2011) 445–451, https://doi.org/10.7937/TCIA.2019.9stoinf1.